

Highly polar phase stabilized at interface of perovskite superlattice designed by oxygen octahedron rotation reconstruction

Hongwei Wang^{1,5}, Jianguo Wen^{2,*}, Dean J. Miller², Qibin Zhou⁴, Ho Nyung Lee³, Karin M. Rabe⁴, and Xifan Wu^{1,*}

¹Department of Physics, Temple University, Philadelphia, PA 19122, USA

²Electron Microscopy Center - Center for Nanoscale Materials, Argonne National Laboratory, Argonne, IL 60439, USA

³Materials Science and Technology Division, Oak Ridge National Laboratory, Oak Ridge, Tennessee 37831, USA

⁴Department of Physics and Astronomy, Rutgers University, Piscataway, NJ 08854-8019, USA and

⁵Department of Materials Science and Engineering, Drexel University, Philadelphia, PA 19104, USA

Ferroelectricity (FE) is generally suppressed in $Pbnm$ structured perovskite such as CaTiO_3 (CTO) [1]. Notably, large FE is favored in perovskite of $R3c$ structure like BiFeO_3 [2], which is a metastable phase of CTO. Here, we report the stabilization of the highly-polar $R3c$ -like phase of CTO in the BaTiO_3 (BTO)/CTO superlattice grown on a SrTiO_3 (STO) substrate. Through a combination of amplitude-contrast sub 0.1nm high-resolution transmission electron microscopy (HRTEM) and first-principles calculations of the structure, energetics, and polarization of the superlattice and its constituents, the above is found to be realized by a reconstruction of the oxygen octahedron rotations at the interfaces from the pattern in nonpolar bulk CTO to a different pattern that is characteristic of a metastable $R3c$ phase of CTO. Under this new mechanism, a large number of perovskites with the CTO structure type, which include many magnetic representatives, are now good candidates for novel highly-polar multiferroic materials [3].

Novel mechanisms for ferroelectricity have recently been the subject of active research, both for their fundamental scientific interest and the technological importance of ferroelectrics and related materials [4]. Novel ferroelectrics have potentially higher performance for particular applications, as well as potential compatibility with other functional properties such as magnetism, yielding multiferroics and other multifunctional materials [3, 5, 6].

Artificially structured perovskite superlattices offer rich opportunities for novel ferroelectricity [7–11]. Non-bulk phases for the constituent layers can be stabilized by the mechanical and electrical boundary conditions characteristic of the superlattice [12, 13], potentially turning constituents that are nonpolar in bulk form into ferroelectrics [14, 15]. Competing low-energy metastable phases can be readily found in perovskites with low tolerance factors, promoting oxygen octahedron rotation instabilities along the Brillouin-zone-boundary R-M line. The ground state structure in such cases is generally the nonpolar orthorhombic $Pbnm$ structure ($a^-a^-c^+$ in Glazer notation) [1]. For many systems, a different rotation pattern ($a^-a^-a^-$) yields a low-energy metastable structure [1], with a large polarization along (111); for BiFeO_3 this $R3c$ structure is in fact the ground state [2]. Depending on the structural energetics of the particular materials, the mismatch epitaxial strain mechanical boundary condition and uniform displacement field electrical boundary condition could stabilize this metastable phase for the entire constituent layers or in a region near in the interface.

With the development of a spherical-aberration (Cs)

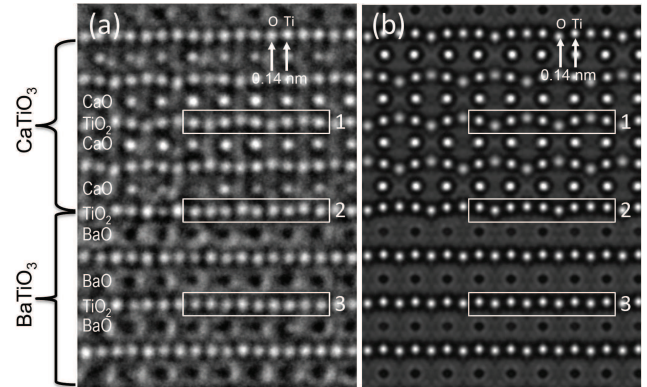


FIG. 1: **Experimental and simulated HRTEM images showing oxygen octahedral tilts in the 4BTO/4CTO superlattice film grown on an STO substrate along [110].** (a). Experimental HRTEM image using an amplitude contrast imaging method ($C_s = 3\mu\text{m}$, $C_c = 1\mu\text{m}$, $\Delta f = -1\text{nm}$). BaO columns (dark dots) and CaO columns (bright dots) show different channeling contrast. Oxygen atomic columns displace differently upward and downward with respect to the central Ti atoms in box 1, 2 and 3. (b). Simulated HRTEM image using the atomic positions obtained from first-principles calculations.

corrector, aberration-corrected HRTEM is a powerful method for accurate visualization of oxygen octahedron distortions [16, 17]. More recently, it was shown that the amplitude contrast imaging in HRTEM could be used also to discriminate heavy and light element columns based on the channeling contrast [18], allowing us to locate the exact interface and to visualize oxygen octa-

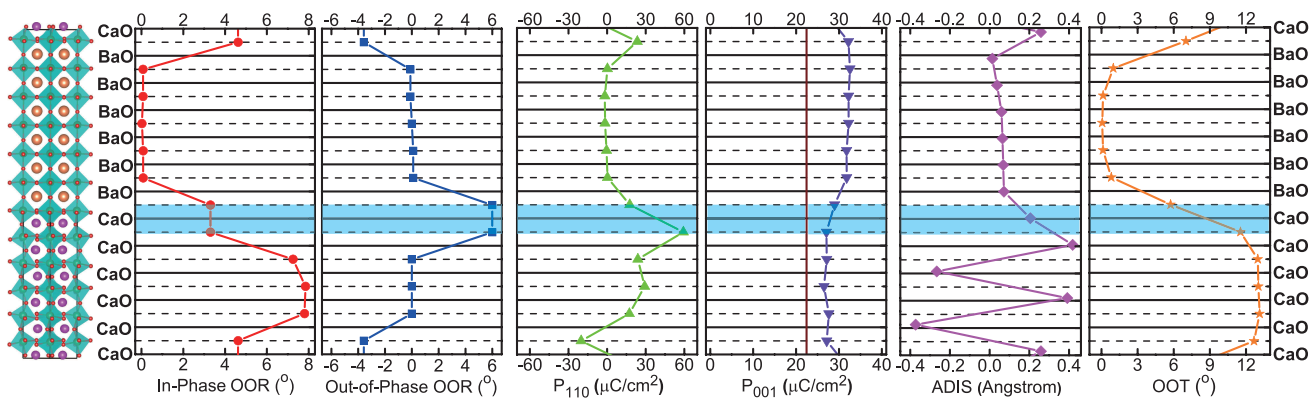


FIG. 2: **Computed local properties associated with ferroelectric and non-polar modes in 6BTO/6CTO superlattice.** First-principles calculations of 6BTO/6CTO superlattice showing layer-by-layer decompositions of in-phase OOR, out-of-phase OOR, in-plane polarization P_{110} , out-of-plane polarization P_{001} , A-site cation displacements (ADIS), and OOT. A highly polar interface phase of one unit cell of CTO (highlighted in blue) is characterized by OOT and out-of-phase OOR)

hedron tilt (OOT) angles in different atomic layers (see Supplementary Materials S1). Fig. 1(a) shows an experimental cross-sectional HRTEM image of a 4BTO/4CTO superlattice film along the $[110]$ direction of the STO substrate obtained by correcting both spherical and chromatic aberrations under typical amplitude contrast imaging conditions ($C_s = 3 \mu\text{m}$, $C_c = 1 \mu\text{m}$). In this image, channeling contrast between Ca and Ba columns is clearly observed: atomic columns of CaO and BaO appear as bright and dark dots, respectively; oxygen and Ti columns appear as bright dots. It can be seen that BTO and CTO coherently grow on the STO substrate, showing the same in-plane lattice constant as that of STO, and elongated c -axis in the BTO layer and shortened c -axis in the CTO layer (see Supplementary Materials S2). Within the CTO layer of the superlattice (box 1), a strongly corrugated TiO_2 plane is observed in which the oxygen atoms displace upward and downward with respect to the central Ti atoms, corresponding to an OOT around $[110]$ by 9° , comparable to that of bulk CTO. For TiO_2 planes between two BaO planes (box 3), alternating displacement of the oxygen atoms, and thus the amplitude of the OOT, is negligible, consistent with the fact that bulk BTO strongly resists oxygen octahedron rotations and tilts. For TiO_2 planes between one BaO and one CaO plane (box 2), the OOT amplitude is 3° , smaller than that in the interior of the CTO layer.

For comparison, in Fig. 1(b) we present the simulated HRTEM image for the atomic positions of the 4BTO/4CTO superlattice obtained from first-principles calculations. The simulated HRTEM image for the computed structure shows the same pattern of OOT as in the experiment (compare boxes 1, 2, and 3 in Fig. 1(a) and (b)), with amplitudes of 12.5° in the CTO layer and 5.5° at the interface. The quantitative difference in OOT angles from the experimental observation can be partly attributed to the fact that the experiments were performed

at $T = 300 \text{ K}$, while the structure relaxation by DFT is for the $T = 0 \text{ K}$ ground state. In addition, in this image it is possible to discern the small uniform displacement of the oxygens relative to the Ti atoms in the TiO_2 plane, which is associated with the spontaneous polarization of the superlattice. While this displacement is present in all the TiO_2 layers, it can be more easily identified in those belonging to the interior BTO layers, which do not have the corrugation associated with OOT.

We use the atomic-scale information from the first-principles results for a detailed investigation of the structure and properties of the superlattice, decomposed layer by layer. We focus our discussion on the 6BTO/6CTO superlattice, which allows a clearer distinction between the interface and interior layers; the corresponding results for the 4BTO/4CTO superlattice can be found in the Supplementary Materials S4. The computed spontaneous polarization is $29 \mu\text{Ccm}^{-2}$ along $[001]$ and $11 \mu\text{Ccm}^{-2}$ along $[110]$. The layer-by-layer decomposed structural distortions and polarizations are shown in Fig. 2.

According to the dielectric slab model of Ref. [14], the structure of constituent layers of the superlattice should be closely related to those of strained bulk materials under the electrical and mechanical boundary conditions imposed by the superlattice. Indeed, as shown in Fig. 2, the interior BTO layers have negligible OOT and oxygen octahedron rotation (OOR) with a polarization of $32 \mu\text{C}/\text{cm}^2$ along $[001]$ direction. This is consistent with the structure and large polarization of strained BTO; the reduction from the strained bulk value of $42 \mu\text{C}/\text{cm}^2$ can be attributed to the electrostatic cost of polarizing the nonpolar CTO layer. Strained CTO is characterized by the same strong oxygen octahedron rotations and tilts as bulk CTO, originating from instabilities at the zone-boundary M and R points, respectively. Therefore, the interior CTO layers are dominated by in-phase OOR and

OOT as can be seen in Fig. 2. An additional distortion present in bulk and strained CTO is a very large A-site displacement, alternating from plane to plane. This X-point mode is induced by the in-phase OOR and OOT distortions through a tri-linear coupling term. This distortion in the interior CTO layers can be clearly seen in Fig. 2, as well as in the TEM image in Fig. 1 (a) (see Supplementary Materials S3). Due to the applied tensile epitaxial strain, the interior CTO layers are polar along [110] direction with a magnitude of $26.4\mu\text{C}/\text{cm}^2$ just like the strained CTO [19].

If the effect of interfaces is negligible, the dielectric slab model can be used to predict the polarization, yielding a value of $22.4\mu\text{C}/\text{cm}^2$ along the [001] direction. However, the first-principles calculation gives $P_{001} = 29.0\mu\text{C}/\text{cm}^2$. Such a large enhancement of the polarization ($\sim 25\%$) is a strong indication of a highly polar interface reconstruction. Indeed, examination of Fig. 2 reveals that the structure of interface CTO layers differs significantly from that of the strained bulk, with the OOT as well as the in-phase OOR being strongly suppressed. The A-site displacement, which is driven by the OOT and in-phase OOR through tri-linear coupling term, is suppressed too. Furthermore, a new structural feature emerges at the interface: an out-of-phase OOR for a TiO_6 sandwiched between two interface CaO layers, with rotation angles comparable to those of the strained bulk in-phase OOR.

Here, we propose that this change in structure at the interface can be interpreted as the local stabilization of a metastable CTO phase with a structure different from that of the bulk. Instead of in-phase OOR, the OOT of this metastable phase is coupled with an out-of-phase OOR around [001]. The out-of-phase OOR originates from the R point instability of the Brillouin zone. This change in the pattern of oxygen octahedron distortions is compatible with a large polarization; this epitaxially strained phase is derived from the metastable polar $e\text{-}R3c$ phase, which is 66.2 meV/fu higher in energy and has a computed polarization along [111] of magnitude $45.5\mu\text{C}/\text{cm}^2$ [1, 20]. It has been shown that this phase cannot be stabilized relative to the $Pbnm$ phase by epitaxial strain alone [20]. However, in the superlattice with BTO, the suppression of the tilt angles by proximity to BTO, assisted by the electrical and mechanical boundary conditions that favor a phase with a component of polarization along [001], is sufficient to stabilize the structure in the present case [21].

To explore the stabilization of this phase more quantitatively, we constructed first-principles-based models for the strained $Pbnm$ phase (designated LP for low polarization phase) and for the metastable $e\text{-}R3c$ phase (designated HP for high polarization phase): $E_{\text{LP}}(M, R_{xy}, X, \Gamma_{xy})$ and $E_{\text{HP}}(R_z, R_{xy}, \Gamma_{xy}, \Gamma_z)$. The models of both E_{LP} and E_{HP} are built through polynomial expansion of the total energy from first-principles calculations with respect to the high-symmetry reference

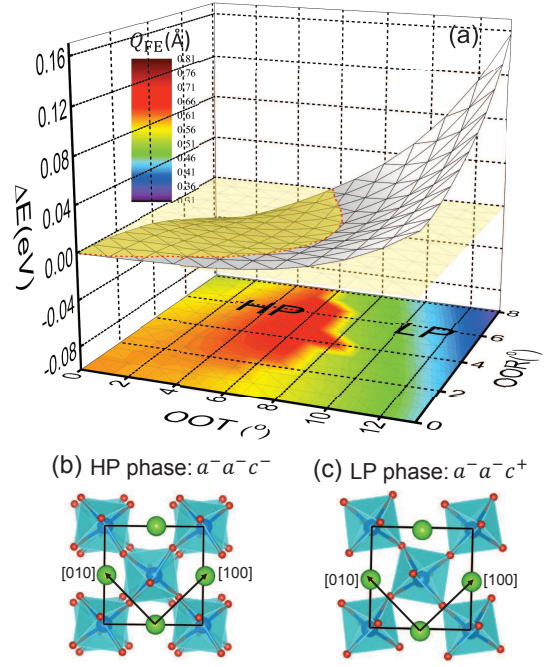


FIG. 3: Phase stabilities of high polarization (HP) and low polarization (LP) phase as functions of oxygen octahedral tilt and rotation. (a) Relative energetics between HP and LP phase as plotted by ΔE as functions of OOR and OOT angles. The FE mode amplitudes are represented by projected colors in the XY plane. (b) and (c) denote the schematic octahedral rotations in HP and LP phase respectively.

structure with $P4/mmm$ symmetry in the amplitudes of the relevant modes. In the above, $M, R_z, R_{xy}, X, \Gamma_{xy}, \Gamma_z$ represent the mode amplitude of in-phase OOR, out-of-phase OOR, OOT, anti-polar mode, and FE modes in [110] and [001] direction respectively. The resulting models are shown in the following for E_{LP} and E_{HP} respectively as (see Supplementary Materials S5 for fitted coefficients):

$$\begin{aligned}
 E_{\text{LP}} = & a_1 M^2 + b_1 M^4 + a_2 R_{xy}^2 + b_2 R_{xy}^4 + a_3 X^2 + b_3 X^4 \\
 & + a_4 \Gamma_{xy}^2 + b_4 \Gamma_{xy}^4 + c_1 M^2 R_{xy}^2 + c_2 M^2 X^2 \\
 & + c_3 M^2 \Gamma_{xy}^2 + c_4 R_{xy}^2 X^2 + c_5 R_{xy}^2 \Gamma_{xy}^2 + c_6 X^2 \Gamma_{xy}^2 \\
 & + d_1 M R_{xy} X,
 \end{aligned} \tag{1}$$

$$\begin{aligned}
 E_{\text{HP}} = & \alpha_1 R_z^2 + \beta_1 R_z^4 + \alpha_2 R_{xy}^2 + \beta_2 R_{xy}^4 + \alpha_3 \Gamma_z^2 \\
 & + \beta_3 \Gamma_z^4 + \alpha_4 \Gamma_{xy}^2 + \beta_4 \Gamma_{xy}^4 + \gamma_1 R_z^2 R_{xy}^2 + \gamma_2 R_z^2 \Gamma_z^2 \\
 & + \gamma_3 R_z^2 \Gamma_{xy}^2 + \gamma_4 R_{xy}^2 \Gamma_z^2 + \gamma_5 R_{xy}^2 \Gamma_{xy}^2 + \gamma_6 \Gamma_z^2 \Gamma_{xy}^2 \\
 & + \kappa_1 R_z R_{xy} \Gamma_z \Gamma_{xy}.
 \end{aligned} \tag{2}$$

Assuming the angles of the OOR and OOT are tunable parameters under experimental conditions, we further define the functions $\mathcal{F}_{\text{LP}}(M, R_{xy}) = \min_{X, \Gamma_{xy}} E_{\text{LP}}(M, R_{xy}, X, \Gamma_{xy})$, and

$\mathcal{F}_{\text{HP}}(\mathbf{R}_z, \mathbf{R}_{xy}) = \min_{\Gamma_{xy}, \Gamma_z} E_{\text{HP}}(\mathbf{R}_z, \mathbf{R}_{xy}, \Gamma_{xy}, \Gamma_z)$. In order to understand how the HP phase can be stabilized relative to the LP phase, we then evaluate $\Delta E = \mathcal{F}_{\text{HP}} - \mathcal{F}_{\text{LP}}$ as functions of OOR and OOT angles. The resulting ΔE is presented in Fig. 3(a) and the FE mode amplitudes are also shown in the color spectrum in the base plane. It can be seen that when the angles are fixed to their values of strained bulk ground state ($\angle\text{OOR} = 8.3^\circ$ and $\angle\text{OOT} = 12.6^\circ$), the LP phase is strongly favored in energy. In the LP phase, the antipolar distortion instead of the FE distortion is favored according to the large tri-linear coupling term $\sim d_1 \text{MR}_{xy}X$ in Eq. 1. Notably, when the amplitudes of oxygen octahedron distortions particularly the OOT are reduced, the HP phase instead of LP phase becomes energetically more stable as schematically shown in Fig. 3(b) and (c) respectively. It strongly indicates that the HP phase can be stabilized over the LP phase when the OOT is reduced. In addition to the change of collective oxygen octahedral distortions, the HP phase is found to have generally much larger FE mode amplitudes than those in the LP phase. The much stronger FE polarization is expected originating from the *e-R3c* phase; it can also be easily understood by the large four-linear coupling term $\sim \kappa_1 \mathbf{R}_z \mathbf{R}_{xy} \Gamma_z \Gamma_{xy}$, in which the collective distortions of out-of-phase OOR and OOT are promoting the FE in both the in-plane and out-of-plane directions.

The HP phase is exactly the highly polar interface phase that occurs at the interface of the BTO/CTO superlattice. Assuming the octahedra to be fairly rigid, the reduction of OOT is imposed by the adjoining BTO layer, which is strongly resistant to the OOT distortion. A direct consequence of the stabilization of the HP structure at the interface is that the polarization of the superlattice is greatly enhanced. For a particular choice of angles with $\angle\text{OOR} = 5.7^\circ$ and $\angle\text{OOT} = 6.6^\circ$ similar to those in the superlattice, the computed polarization of the HP phase is over $54.0 \mu\text{C}/\text{cm}^2$, which is comparable to the polarization of $45.5 \mu\text{C}/\text{cm}^2$ in the bulk *e-R3c* CTO. In the superlattice, the HP phase is further favored by both the electrostatic and mechanical boundary conditions imposed by the polarization of the BTO layer according to Eq. 2. Under the continuous displacement field along [001] direction, the electrostatic boundary condition tends to depolarize the strained BTO layers and polarize the CTO including both strained bulk and interface parts with a larger Γ_z , i.e. FE along [001] direction. Under the tensile strain due to the mismatch between STO and CTO, the mechanical boundary condition effectively enhances Γ_{xy} , i.e. FE along [110] direction.

A unique effect emerges from the stabilization of the HP phase in the superlattices, in that the interface enhances the polarization. As shown in Fig. 4, we computed the in-plane P_{110} , out-of-plane P_{001} , and total polarizations P_{total} of the superlattices as a function of n

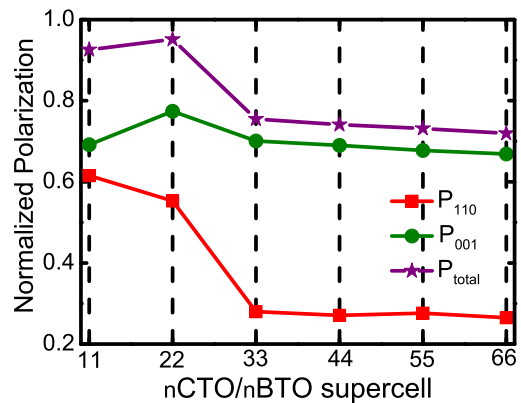


FIG. 4: **Polarization as a function of interface density.** In-plane polarization P_{110} , out-of-plane polarization P_{001} , and total polarization P_{total} as a function of n in $n\text{BTO}/n\text{CTO}$ supercells.

in $n\text{BTO}/n\text{CTO}$ supercells. Indeed, when the interface become more dense with smaller n in $n\text{BTO}/n\text{CTO}$ supercells, the overall polarization P_{001} along [001] direction increases. The maximum polarization is achieved in $2\text{BTO}/2\text{CTO}$ supercell. This is expected since the stabilized HP phase will require the collective motion of two interface CTO layers. In $2\text{BTO}/2\text{CTO}$, the induced HP phase can be unambiguously identified by the anomalously large polarization P_{110} , which in turn pushes up the P_{001} by the four-linear coupling term in Eq. 2. This is contrary to the conventionally expected negative dipole moment induced at the interface suppressing the overall FE of the superlattice. This unusual behavior has been reported in theoretical calculations [21, 22], while the physical origin is first elucidated in this work.

By combining HRTEM experimental technique and first-principles theory, we introduced a comprehensive interface design method to stabilize a highly polar metastable phase, as well as careful considerations of both electric and mechanical boundary conditions. Given that the OOT and OOR are general properties in perovskite, our approach can be broadly applied on the other perovskite materials to achieve enhanced polarization or closely related properties. Furthermore, the result of our current work indicates that, through an interface design mechanism, short-period superlattice can have stronger FE than longer ones. This is promising for modern device applications based on ultra-thin films.

METHODS

Thin Film Growth: Atomic-scale BTO/CTO superlattice films were synthesized on STO (001) single-crystalline substrates using pulsed laser deposition equipped with reflection high-energy electron diffraction. For electrical characterization, epitaxial SrRuO_3 con-

ducting thin films were deposited as bottom electrodes with preserved single terrace steps ($\sim 0.4nm$) on STO substrates. BTO and CTO layers were then deposited with a total film thickness of about $200nm$.

TEM: High-resolution transmission electron microscopy (HRTEM) was carried out using the Argonne Chromatic Aberration-Corrected TEM (ACAT) at $200kV$. HRTEM images were taken under amplitude contrast imaging conditions with spherical and chromatic aberration less than $3\mu m$ and $1\mu m$ respectively. Cross-sectional TEM specimens were prepared using the focused ion beam approach followed by low-energy Ar ion polishing.

First-principles Calculations: First-principles total-energy calculations were performed by density functional theory as implemented in the Vienna *ab initio* simulations package (VASP) [23]. The nBTO/nCTO ($n = 1, \dots, 6$) superlattices were modeled by the $\sqrt{2}a \times \sqrt{2}a \times c$ supercell under periodic boundary conditions. The epitaxial strain was considered by fixing the in-plane lattice constant to be that of theoretically relaxed cubic SrTiO₃(STO) ($a = 3.90\text{\AA}$), while the c lattice constants were allowed to relax. We used the Perdew-Burke-Ernzerhof functional revised for solids [24]. The projector-augmented wave method was used with the following valence-electron configurations: $5s^25p^66s^2$ for Ba, $3s^23p^64s^2$ for Ca, $3p^64s^13d^3$ for Ti, and $2s^22p^4$ for O. The kinetic-energy cutoff for the plane-wave basis was 500 eV , total energy convergence accuracy was 10^{-8} eV . The atomic positions were considered to be fully relaxed when the residual force was less than $1\text{meV}/\text{\AA}$. We used a $6 \times 6 \times 4$ k -point mesh for 1BTO/1CTO as well as bulk and strained CTO, $6 \times 6 \times 2$ and $6 \times 6 \times 1$ mesh k -points for 2BTO/2CTO and nBTO/nCTO ($n = 3, \dots, 6$) respectively. For strained BTO, a $6 \times 6 \times 6$ k -points sampling was used. The spontaneous polarization was calculated by the Berry phase formalism based on modern theory of polarization [25]. The local polarization profile was computed based on linear response theory involving the effective charge approximation [26] and small ionic distortions from high symmetry structure. Our group theoretical analyses were carried out with the aid of the ISOTROPY programs [27].

First-principles-based modeling of the structural energetics of the ground-state phase of CTO, as well as a metastable phase to be discussed further below, was carried out through polynomial expansion of the total energy with respect to a high-symmetry centro-symmetric reference structure with $P4/mmm$ symmetry in the amplitudes of the relevant modes. The out-of-plane lattice constants c are fixed at the lattice constant of strained bulk with the in-plane lattice constant is fixed to be the theoretical lattice constant of cubic STO. Coefficients are determined based on the computed total energy for configurations obtained by freezing in individual modes and combinations of modes.

ACKNOWLEDGMENTS

X. W. was supported as part of the Center for the Computational Design of Functional Layered Materials, an Energy Frontier Research Center funded by the U.S. Department of Energy, Office of Science, Basic Energy Sciences under Award no. de-sc0012575. The work of K. M. R. was supported by NSF DMR-1334428. This research used resources of the National Energy Research Scientific Computing Center (NERSC), a DOE Office of Science User Facility supported by the Office of Science of the U.S. Department of Energy under Contract No. DE-AC02-05CH11231. The transmission electron microscopy was accomplished at the Electron Microscopy Center Center for Nanoscale Materials at Argonne National Laboratory, a DOE-BES Facility supported under Contract DE-AC02-06CH11357 by UChicago Argonne, LLC. The work at ORNL was supported by the U.S. Department of Energy, Office of Science, Basic Energy Sciences, Materials Sciences and Engineering Division.

-
- [1] Benedek, N. A. & Fennie, C. Why are there so few perovskite ferroelectrics? *J. Phys. Chem. C* **117**, 13339-13349 (2013).
 - [2] Neaton, J. B., Ederer, C., Waghmare, U. V., Spaldin, N. A. & Rabe, K. M. First-principles study of spontaneous polarization in multiferroic BiFeO₃. *Phys. Rev. B* **71**, 014113 (2005).
 - [3] Spaldin, N. A., Cheong, S. W. & Ramesh, R. Multiferroics: Past, present, and future. *Phys. Today* **63**, 38 (2010).
 - [4] Dawber, M., Rabe, K. M. & Scott, J. F. Physics of thin-film ferroelectric oxides. *Rev. Mod. Phys.* **77**, 1083-1130 (2005).
 - [5] Lee, J. H. *et al.* A strong ferroelectric ferromagnet created by means of spin-lattice coupling. *Nature* **466**, 954 (2010).
 - [6] Benedek, N. A. & Fennie, C. Hybrid improper ferroelectricity: A mechanism for controllable polarization-magnetization coupling. *Phys. Rev. Lett.* **106**, 107204 (2011).
 - [7] Ahn, C. H., Rabe, K. M. & Triscone, J. M. Ferroelectricity at the nanoscale: Local polarization in oxide thin films and heterostructures. *Science* **303**, 488-491 (2004).
 - [8] Lee, H. N., Christen, H. M., Chisholm, M. F., Rouleau, C. M. & Lowndes, D. H. Strong polarization enhancement in asymmetric three-component ferroelectric superlattices. *Nature* **433**, 395-399 (2005).
 - [9] Warusawithana, M. P., Colla, E. V., Eckstein, J. N. & Weissman, M. B. Artificial dielectric superlattices with broken inversion symmetry. *Phys. Rev. Lett.* **90**, 036802 (2003).
 - [10] Sai, N., Meyer, B. & Vanderbilt, D. Compositional inversion symmetry breaking in ferroelectric perovskites. *Phys. Rev. Lett.* **84**, 5636-5639 (2000).
 - [11] Bousquet, E., Dawber, M., Stucki, N., Lichtensteiger, C., Hermet, P., Gariglio, S., Triscone, J. & Ghosez, P.

- Improper ferroelectricity in perovskite oxide artificial superlattices. *Nature* **452**, 732-737 (2008).
- [12] Schlom, D. G., Chen, L. Q. & Eom, C. B. *et al.* Strain tuning of ferroelectric thin films. *Annu. Rev. Mater. Res.* **37**, 589-626 (2007).
- [13] Stengel, M., Spaldin, N. A. & Vanderbilt, D. Electric displacement as the fundamental variable in electronic-structure calculations. *Nature Phys.* **5**, 304-308 (2009).
- [14] Neaton, J. B. & Rabe, K. M. Theory of polarization enhancement in epitaxial BaTiO₃/SrTiO₃ superlattices. *Appl. Phys. Lett.* **82**, 1586-1588 (2003).
- [15] Jang, H. W. *et al.* Ferroelectricity in strain-free SrTiO₃ thin films. *Phys. Rev. Lett.* **104**, 197601 (2010).
- [16] Jia, C. L., Lentzen, M. & Urban, K. Atomic-resolution imaging of oxygen in perovskite ceramics. *Science* **299**, 870-873 (2003).
- [17] Jia, C. L., Mi, S. B., Urban, K., Vrejoiu, I., Alexe, M. & Hesse, D. Atomic-scale study of electric dipoles near charged and uncharged domain walls in ferroelectric films. *Nat. Mater.* **7**, 57-61 (2008).
- [18] Wang, A., Chen, F. R., Van Aert, S. & Van Dyck, D. Direct structure inversion from exit waves: Part I: Theory and simulations. *Ultramicroscopy* **110**, 527 (2010).
- [19] Eklund, C. J., Fennie, C. J. & Rabe, K. M. Strain-induced ferroelectricity in orthorhombic CaTiO₃ from first principles. *Phys. Rev. B* **79**, 220101 (2009).
- [20] Eklund, C. J. Interplay of strain, polarization and magnetic ordering in complex oxides from first principles. Ph.D. thesis (Rutgers University, 2010).
- [21] Zhou, Q. First-principles modeling of functional perovskite materials and superlattices. Ph.D. thesis (Rutgers University, 2014).
- [22] Lu, X. Z., Gong, X. G. & Xiang, H. J. Polarization enhancement in perovskite superlattices by oxygen octahedral tilts. *Comput. Mater. Sci.* **91**, 310-314 (2014).
- [23] Kresse, G. & Furthmüller, J. Efficient iterative schemes for ab initio total-energy calculations using a plane-wave basis set. *Phys. Rev. B*, **54**, 11169 (1996).
- [24] Perdew, J. P. *et al.* Restoring the density-gradient expansion for exchange in solids and surfaces. *Phys. Rev. Lett.* **100**, 136406 (2008).
- [25] Marzari, N., Mostofi, A. A., Yates, J. R., Souza, I. & Vanderbilt, D. Maximally localized Wannier functions: Theory and applications. *Rev. Mod. Phys.* **84**, 1419 (2012).
- [26] Meyer, B. & Vanderbilt, D. Ab initio study of ferroelectric domain walls in PbTiO₃. *Phys. Rev. B* **65**, 104111 (2002).
- [27] Stokes, H. T., Hatch, D. M. & Campbell, B. J. ISOTROPY. Brigham Young University: Provo, Utah, 2007.